catalysts

MDPI

Article

3D-Printed Monoliths Based on Cu-Exchanged SSZ-13 as Catalyst for SCR of NO_x

Elisabetta M. Cepollaro [1], Stefano Cimino [1], Marco D'Agostini [2], Nicola Gargiulo [3], Giorgia Franchin [2] and Luciana Lisi [1,*]

[1] Istituto di Scienze e Tecnologie per l'Energia e la Mobilità Sostenibili (STEMS), Consiglio Nazionale delle Ricerche (CNR), Via Guglielmo Marconi 4/10, 80125 Napoli, Italy; elisabettamaria.cepollaro@stems.cnr.it (E.M.C.); stefano.cimino@cnr.it (S.C.)
[2] Dipartimento di Ingegneria Industriale, Università degli Studi di Padova, Via Marzolo 9, 35131 Padova, Italy; marcolorenzo.dagostini@phd.unipd.it (M.D.); giorgia.franchin@unipd.it (G.F.)
[3] Centro Servizi Metrologici e Tecnologici Avanzati (CeSMA), Università di Napoli Federico II, Corso N. Protopisani, 80146 Napoli, Italy; ngargiul@unina.it
* Correspondence: luciana.lisi@cnr.it; Tel.: +39-081-7682279

Abstract: Monoliths manufactured by Direct Ink Writing containing 60% SSZ-13 (SiO_2/Al_2O_3 = 23) and SiO_2 with 10% laponite as a binder were investigated as self-standing structured catalysts for NH_3-SCR of NO_x after a short (4 h) and prolonged (24 h) ion exchange with copper and then compared with pure SSZ-13 exchanged under the same conditions. The catalysts were characterized by morphological (XRD and SEM), textural (BET and pore size distribution), chemical (ICP-MS), redox (H_2-TPR), and surface (NH_3-TPD) analyses. The silica-based binder uniformly covered the SSZ-13 particles, and copper was uniformly distributed as well. The main features of the pure Cu-exchanged SSZ-13 zeolite were preserved in the composite monoliths with a negligible contribution of the binder fraction. NH_3-SCR tests, carried out on both monolithic and powdered samples in the temperature range of 70–550 °C, showed that composite monoliths provided very good activity, and that the intrinsic activity of SSZ-13 was enhanced by the hierarchical structure of the composite material.

Keywords: structured catalysts; additive manufacturing; SSZ-13; $deNO_x$

Citation: Cepollaro, E.M.; Cimino, S.; D'Agostini, M.; Gargiulo, N.; Franchin, G.; Lisi, L. 3D-Printed Monoliths Based on Cu-Exchanged SSZ-13 as Catalyst for SCR of NO_x. *Catalysts* **2024**, *14*, 85. https://doi.org/10.3390/catal14010085

Academic Editor: Anker Degn Jensen

Received: 27 December 2023
Revised: 15 January 2024
Accepted: 17 January 2024
Published: 19 January 2024

1. Introduction

NH_3 Selective Catalytic Reduction (SCR) is the current preferred technology to remove nitrogen oxides (NO_x) from lean-burn diesel engine exhausts, using base metal-exchanged zeolite catalysts (e.g., Cu, Fe) [1]. The SCR section is usually located downstream from the diesel particulate filter (DPF) where the temperature could reach up to 650 °C. Therefore, the SCR catalyst can be easily damaged in the presence of steam generated from the combustion of diesel fuel [2,3].

The more common vanadium-based catalysts have a low hydrothermal stability and poor resistance to alkali metal, whilst zeolite-based catalysts are more tolerant to high temperatures and show a good resistance to alkali metal poisoning due to their high surface area and strong acidity, which makes the zeolite-based catalysts also suitable for $deNO_x$ in flue gas cleaning from biomass-fired applications [4].

Small-pore zeolites such as Cu-SSZ-13 have better NH_3-SCR performance due to the high concentration of active sites, higher hydrothermal stability, poisoning tolerance, and better N_2 selectivity than other zeolites. This last feature is related to the peculiar small-pore structure which limits the generation of undesired byproducts, such as N_2O, having a size larger than the 8-ring (~3.8 Å) [5]. Furthermore, the small-pore structure inhibits the dealumination of the framework and the accumulation of copper species during hydrothermal aging, and the shape selectivity of this small-pore zeolite also prevents long-chain hydrocarbons that could be present in diesel exhaust gases from entering [3]. For

these reasons, this zeolite is presently the most popular NH_3-SCR catalyst in diesel exhaust purification [6,7].

Like all the zeolites with CHA topology, SSZ-13 shows a three-dimensional pore system, which is formed by stacking a hexagonal array of planar 6-membered rings (6-MRs) connected through an AABBCC scheme. Such stacking forms large chabazite cages, whose access is limited by symmetric 8-MRs (diameter: ~0.38 nm) [8]. In copper-exchanged SSZ-13, Cu ions are located in two different extra-reticular sites; indeed, the species labelled as Cu^{2+}-2Z is located in the plane of the 6-MRs, while the species labelled as $[Cu(OH)]^+$-Z is located in the 8-MR-sized window of the CHA cage [9,10]. Both species are considered as active centres for SCR reaction, although Cu^{2+}-2Z is inferred to be less active than $[Cu(OH)]^+$-Z for low-temperature SCR [9]. Cu^{2+}-2Z species prevail in zeolites with a high content of framework Al (Si/Al = 6), whereas in zeolites with low Al content (Si/Al = 35), i.e., zeolites having a low concentration of paired Al (Al atoms separated by one or two Si atoms), the main active copper species is $[Cu(OH)]^+$-Z because the presence of an extra-framework OH ligand enables the stabilization of Cu^{II} cations in the 8-MRs of CHA structure [11]. Indeed, the lack of paired Al arrangements balancing the double positive charge of Cu^{2+}-2Z results in the prevailing of $[Cu(OH)]^+$-Z species in zeolites with a high Si/Al ratio.

However, the Cu^{2+}-2Z species is more hydrothermally resistant [1,9,12] because $[Cu(OH)]^+$-Z species can react with water vapor to form CuO_x clusters. At the same time, water vapor favours the dealumination and subsequent collapse of the zeolite framework due to the formation of $CuAl_2O_4$-like species [9,13]. Moreover, CuO clusters are responsible for NH_3 overoxidation to NO or N_2O in the SCR process [14]. Copper redistribution through the HNO_3 treatment of Cu-SSZ-13 was proposed by Liu et al. [15]. They found that the acid exchange removed the unselective CuO aggregates and, at the same time, increased the fraction of isolated Cu^{2+}. The redistribution of Cu species was caused by the dealumination from outside to inside, providing the sites for the location of Cu^{2+} ions. This resulted in a larger operative SCR temperature window, providing NO_x conversion approaching or equal to 100% from 165 to 690 °C, 100% N_2 selectivity, and a very good resistance to H_2O and SO_2.

The use of purely microporous zeolites for the NH_3-SCR is limited by the slow diffusion of the reactants within a thick catalytic layer and also by the deposition of ammonium nitrates and sulphates in the pores and channels, especially at low temperatures [16]. For this reason, higher performances can be obtained with zeolite catalysts showing a hierarchical porosity. In particular, Chen et al. [17] obtained a hierarchical SSZ-13, adding a mesoporogen agent at the preparation stage in combination with the conventional Structure Directing Agent template (TMAda-OH). Therefore, the dual template method was effective to obtain a bimodal micro/meso-porosity, but also caused the increase in paired Al in the zeolite framework, which in turn promoted the presence of Cu^{2+}-2Z species. Moreover, it was found that the average distance between the framework Al sites in the hierarchical SSZ-13 shortened with increasing contents of the mesoporogen agent.

To obtain technological catalysts for environmental applications treating gas streams, the zeolite-based active phase is generally applied onto a high surface area monolithic (honeycomb) scaffold that guarantees mechanical strength and very low pressure drops [6,7]. In particular, Cu-exchanged SSZ-13 was applied as a wash coat onto cordierite honeycombs via a slurry dip-coating method, which used pseudo-boehmite as binder [18,19]. However, some common drawbacks are related to the limited zeolite loading required to prevent the loss of the active phase and/or to poor adhesion for unmatched thermal expansion behaviour with the monolithic substrate [20,21]. Moreover, conventionally extruded honeycomb monoliths with parallel channels suffer from a lack of radial mixing of reactants.

We recently reported [22,23] the preparation and testing in NH_3-SCR of 3D-printed geopolymer/Cu-ZSM-5 monoliths, possibly providing enhanced performance related to (i) the hierarchical porosity of the composite consisting of a macro-mesoporous (geopoly-

mer) matrix and a microporous material (ZSM-5); (ii) improved radial mixing and mass transfer characteristics of 3D-printed monoliths with respect to standard honeycombs; and (iii) higher volumetric loadings of the active phase (zeolite) and good mechanical properties. In this work, following the same approach, we set out to reproduce this methodology for the better-performing zeolite with CHA topology, thus preparing self-standing structured Cu-SSZ-13 catalysts containing a high fraction of zeolite by the Direct Ink Writing method (DIW, an extrusion-based Additive Manufacturing technique). The paper describes the modification of the original methodology applied to ZSM-5 in [22,23], not trivially replicable for SSZ-13, which required the use of colloidal silica and laponite as the binder for the small-pore zeolite, therefore, still keeping a composite system with hierarchical porosity. The resulting 3D monoliths, having the target zeolite loading and good mechanical properties, were fully characterized and eventually tested for the NH_3-SCR reaction.

2. Results and Discussion

2.1. Catalysts Preparation

The first attempts to replicate the same alkaline slurry previously used for the preparation of geopolymer-ZSM-5 structured composites [22,23] were not successful and caused the almost total loss of the original crystalline structure of the SSZ-13 (Figure 1). This was due to the poor resistance of the SSZ-13 structure to the highly alkaline environment required to synthesize a geopolymer matrix. For this reason, a colloidal silica with the addition of 10% laponite was used as a binder to provide a mechanically resistant interconnecting matrix, keeping together the preformed SSZ-13 grains.

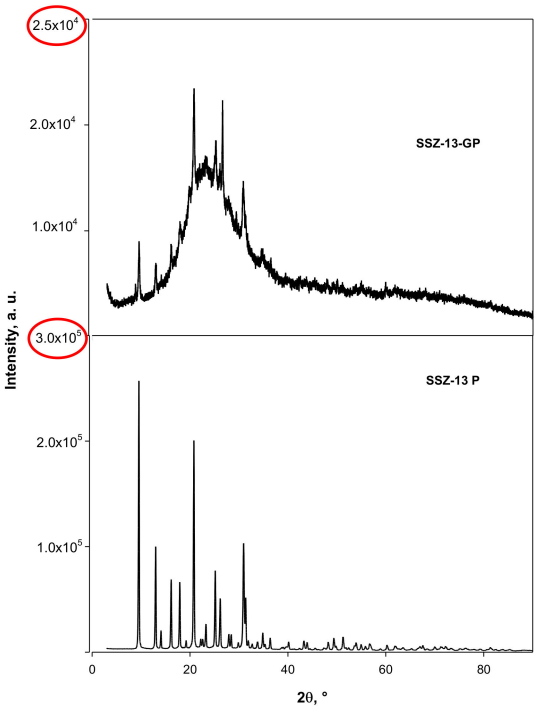

Figure 1. XRD pattern of SSZ-13 (60%) into the geopolymer matrix (**top**) compared with pattern of pure SSZ-13 (**bottom**). Red circles highlight the different order of magnitude of the two scales.

Although using colloidal silica as a binder caused a significant contraction of the structure (diameter of the filaments ranging from 680 to 720 µm) after drying when compared to the geopolymer [23], the subsequent thermal treatment in air at 550 °C produced highly resistant 3D structures with a high mesoporosity. In particular, the addition of 10% laponite clay to the binder proved successful in enhancing the mechanical resistance of the resulting 3D structures (Figure 2) during all the stages of preparation, particularly improving the stability of printed monoliths during drying.

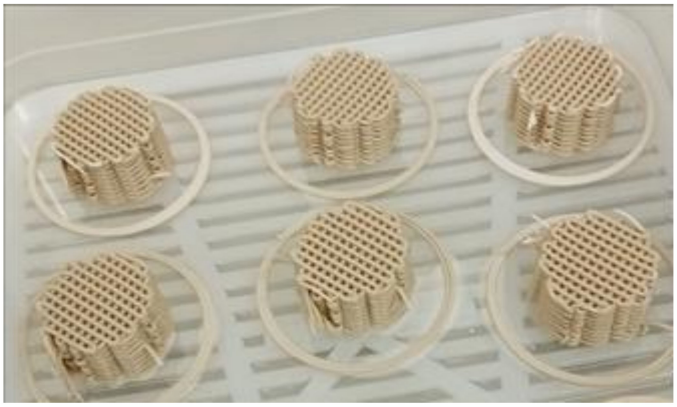

Figure 2. Image of the 3D-printed SSZ-13 monoliths at the end of the synthesis process.

2.2. Catalysts Characterization

As shown in Figure 3, XRD analysis confirmed that the original crystalline structure of the SSZ-13 was completely preserved in the 3D monoliths, using such a formulation of the binder. The small reduction of the intensity of XRD peaks for the monolith sample, with respect to the reference SSZ-13 powder, is purely related to the dilution effect, considering its zeolite loading was fixed at 60 wt%.

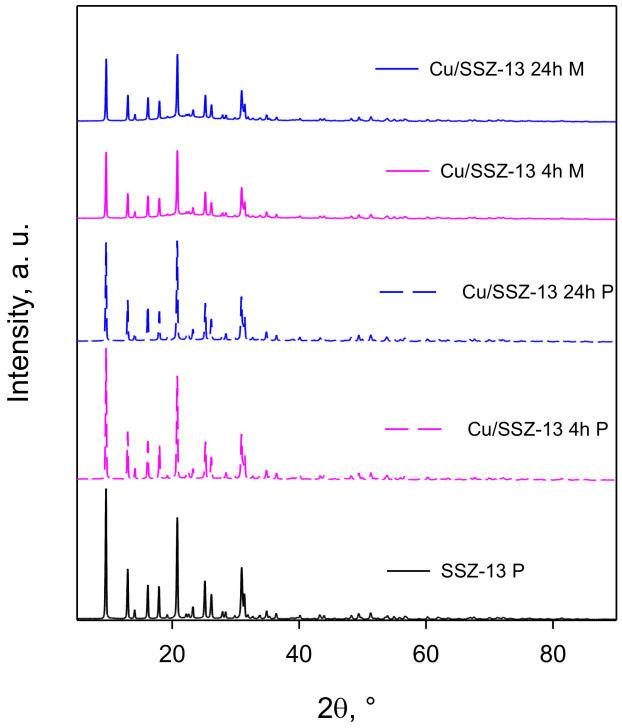

Figure 3. XRD patterns of pure SSZ-13 (black pattern) and Cu-exchanged powder catalysts as well as composite 3D monoliths with 60% SSZ-13 in the silica–laponite matrix.

Ion exchange with copper was performed directly on pre-shaped 3D monoliths after calcination and acid treatment, as described in [22,23]. The visual inspection of the cross section of structured catalysts at the end of preparation showed a uniform blue coloration, suggesting a good penetration of copper throughout the monoliths and a rather uniform distribution of the active metal, excluding any significant confinement of Cu on the external surface, commonly due to the precipitation of the corresponding insoluble hydroxides [22].

Figure 4a–d presents SEM images of 3D-printed composite monoliths at different magnifications.

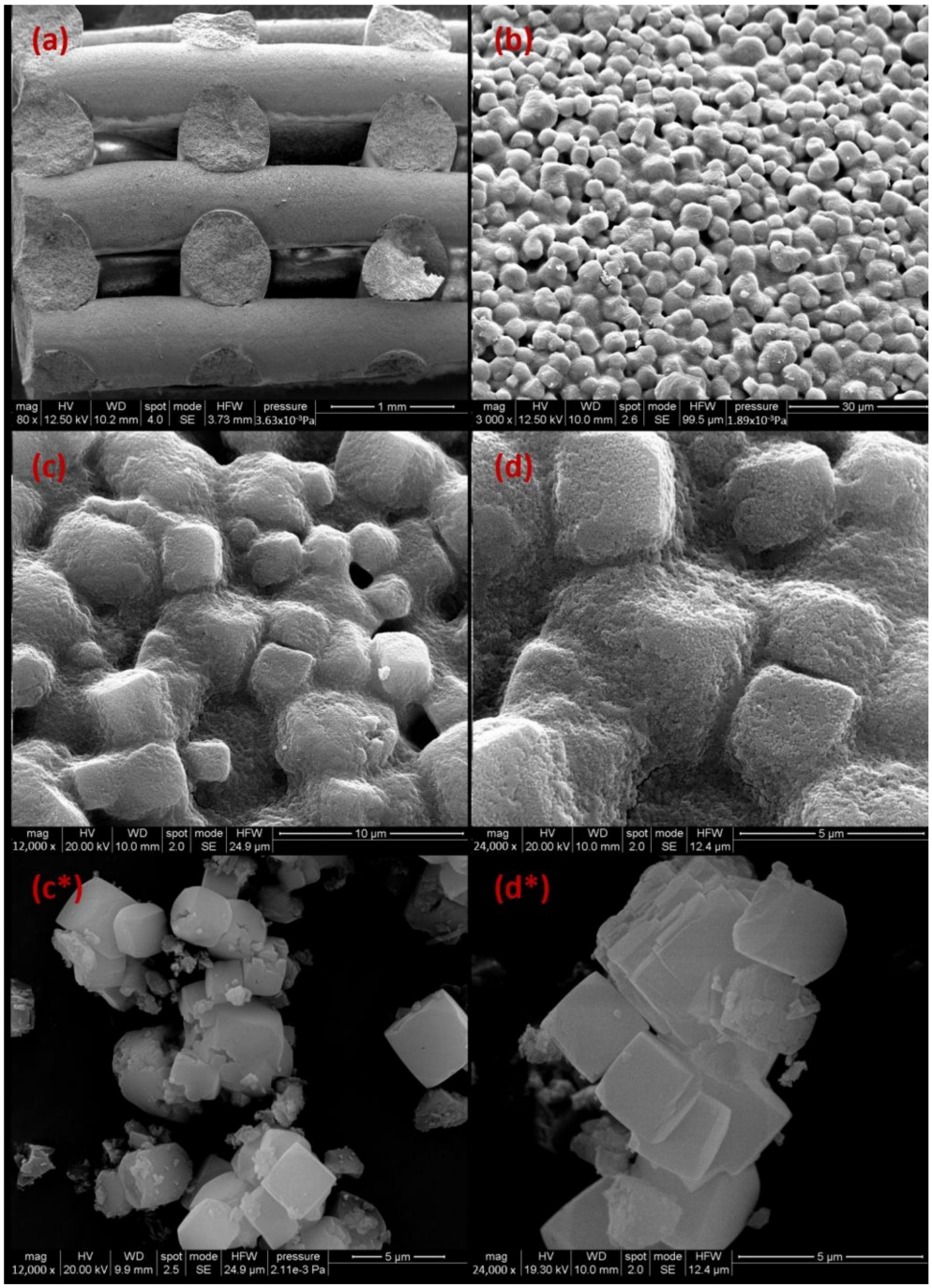

Figure 4. SEM images of 3D-printed SSZ-13 composite monolith at increasing magnification (**a**) (80×), (**b**) (3000×), (**c**) (12,000×), (**d**) (24,000×)) compared with corresponding images of the parent SSZ-13 powder (**c***,**d***) at the same magnification.

Figure 4a highlights the 3D network of the monolith with the filaments with regular diameters (700 ± 20 µm), following a 0–90° sequential build-up to achieve a log-pile scaffold configuration. The filaments are composed of small particles with a cubic morphology and an average size of ≤5 µm (Figure 4b,c), which are completely embedded by a thin film overlayer (Figure 4d) made of much smaller particles. Comparison with the reference SSZ-13 powder (Figure 4c*,d*) confirms that the original morphology and size of the cubic zeolite crystals [17,24] was entirely preserved during the preparation of the 3D-printed monoliths, whereas the colloidal silica binder provided the thin yet firmly anchored interconnecting matrix among crystals.

Figure 5a presents the N_2 adsorption isotherms of both the Cu/SSZ-13 catalyst in powder form and of the 3D-printed composite monolith in comparison with the parent SSZ-13 and the binder. The N_2 physisorption isotherm of the binder calcined for 4 h at 550 °C in air confirmed the typical features of a mesoporous material with a H2 type hysteresis and a disordered interconnected porosity, whereas the isotherms of the two zeolite powders are, as expected, typical of microporous materials [25]. The composite monolith has features of both materials. The corresponding N_2 isotherm shows, in addition to the sharp increase in adsorbed gas at low p/p_0 which is typical of the zeolite, the hysteresis loop of mesoporous materials approaching $p/p_0 = 1$. The fraction and type of pores is reported in Figure 5b, which highlights the absence of micropores for the binder and the decrease in the micropores volume related to the copper exchange. The Cu/SSZ-13 4 h M has a lower fraction of micropores, as expected, due to the lower fraction of SSZ-13 in the composite material and, at the same time, larger mesopores associated with the fraction of the binder. As a matter of fact, the PSD of Cu/SSZ-13 4 h M agrees with the mathematical combination of the PSD of SSZ-13 and that of the binder.

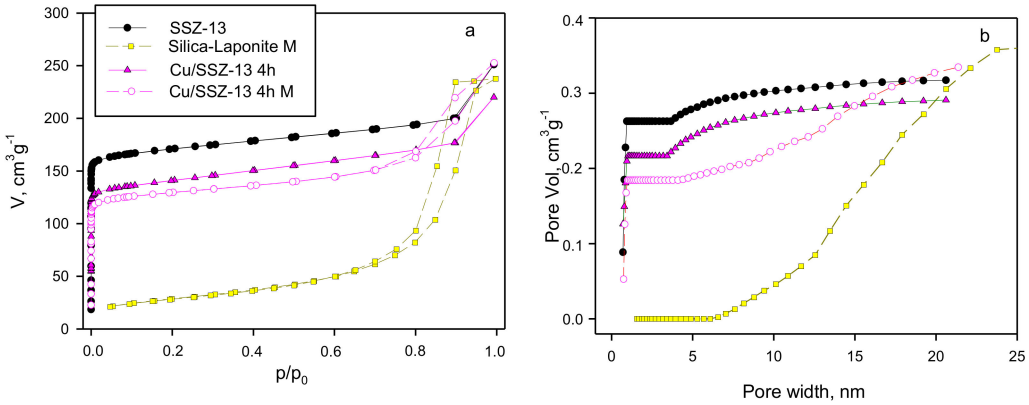

Figure 5. (**a**) N_2 physisorption isotherms and (**b**) cumulative pore size distribution of SSZ-13 powders and monoliths (4 h exchange), compared to the reference SSZ-13 powder and a 3D-printed monolith made of silica + laponite (without any zeolite filler).

On the other hand, the decrease in micropore volume related to copper exchange in the powder zeolites is higher than that expected on the basis of the metal content and should imply the occlusion of some micropores (Table 1).

Table 1. BET-specific surface area, micropore, and total pore volume of powder and monolith catalysts (evaluated by the DFT model and Gurvitch method, respectively).

Sample	Form	BET Area (m^2 g^{-1})	V Micro (cm^3 g^{-1})	V Total (cm^3 g^{-1})
SSZ-13 P	Powder	686	0.26	0.39
SSZ-13 M	3D Monolith	516	0.19	0.35
Cu-SSZ-13 P (4 h)	Powder	557	0.22	0.34
Cu-SSZ-13 M (4 h)	3D Monolith	512	0.18	0.37
Cu-SSZ-13 P (24 h)	Powder	542	0.21	0.30
Cu-SSZ-13 M (24 h)	3D Monolith	463	0.16	0.36

Table 1 reports the corresponding values of the specific surface areas which is evaluated by the BET model, as well as micropores and total volume, calculated by NLDFT model and Gurvitch methods, respectively. After copper exchange and thermal treatment, the BET area of the SSZ-13 zeolite was reduced by only 6%, which mostly corresponds to the effect predicted considering the actual metal loading in the catalyst (Table 2). More-

over, the surface area of the monolith catalyst exceeds the value calculated as the linear combination of the contributions from the two main components (zeolite + silica binder) when considering their actual content in the composite; this suggests a larger porosity of the silica matrix intercalated by the zeolite grains.

Table 2. Copper loading from ICP-MS analysis, H_2 uptake from TPR analysis, and corresponding copper content (assuming a complete Cu^{2+}-Cu^0 reduction); NH_3 amount released during TPD analysis.

Sample	Cu from ICP-MS (wt%)	H_2 Uptake (mmol g^{-1})	Cu Estimated from Total H_2 Uptake (wt%)	Desorbed NH_3 (mmol g^{-1})
SSZ-13 P	-	-	-	3.56
Cu/SSZ-13 P (4 h)	5.09	0.68	4.3	2.65
Cu/SSZ-13 M (4 h)	2.91	0.47	3.0	1.69
Cu/SSZ-13 P (24 h)	6.23	0.95	6.0	2.92
Cu/SSZ-13 M (24 h)	3.33	0.84	5.3	1.86

The comparison of micropores and total pore volume of Cu-exchanged and parent SSZ-13 showed that reduction is mostly assignable to the reduction of micropore volume, where Cu is supposedly located, whereas mesopore volume is much less affected.

The copper loading (by ICP-MS, Table 2) in the zeolite powder and in the 3D monolith after 4 h of ion exchange was equal to 5.1% and 2.9 wt%, respectively. Those values roughly scaled as the zeolite weight content in the composite, confirming that the mesoporous silica matrix does not hinder access of the metal ions to the SSZ micropores. A slight increase in the actual copper loading was achieved by extending the Cu exchange up to 24 h.

The actual copper content was significantly higher than the corresponding theoretical Cation Exchange Capacity (CEC), evaluated on the basis of the SSZ-13 unit cell and its SiO_2/Al_2O_3 ratio, which equals to ca 2.2 wt% Cu, in good agreement with Kwak et al. [26] and Clemens et al. [27]. The contribution of the laponite, having a CEC very close to that of SSZ-13 (0.79 meq/g [28]), is too small to explain the high copper content, and it only occurs for monolith samples. Therefore, it can be argued that the high metal loading is rather associated with the occurrence of an over-exchange phenomenon deriving from the formation Cu-oxo species with different oxygen/Cu ratios (e.g., $[CuO_2Cu]^{2+}$, $[CuOCu]^{2+}$, $[Cu_3O_3]^{2+}$ observed for SSZ-13 with high Si/Al ratio) [29]. However, the formation of extra-framework copper oxides cannot be excluded. In any case, this additional copper is likely also responsible for the partial occlusion of micropores, which is more evident for the pure zeolite sample than for its composite 3D—printed counterpart.

H_2-TPR experiments were used to determine the type and amount of exchanged copper. TPR results are reported in Figure 6, where profiles of Cu-exchanged SSZ-13 powders and monoliths are compared for the two exchange times. It was verified that the parent SSZ-13 powder does not give any contribution to reduction that, consequently, can be assigned only to copper in the metal-exchanged materials. Both TPR profiles of powder and monoliths exchanged for 4 h show similar features with two main signals: the first one, peaking at 252–260 °C, is sharper than the second one, reaching its peak at 501 °C and 575 °C, respectively, for the composite monolith and the powder catalyst. Increasing the Cu loading by extending the exchange time up to 24 h shifted the second reduction peak towards lower temperatures (475 °C and 520 °C, respectively, for monolith and powder). Moreover, it caused the appearance of an additional intermediate peak (at 318 °C and 340 °C), which was particularly evident for the powder sample and suggests the formation of novel copper species that cannot be associated with the presence of the binder.

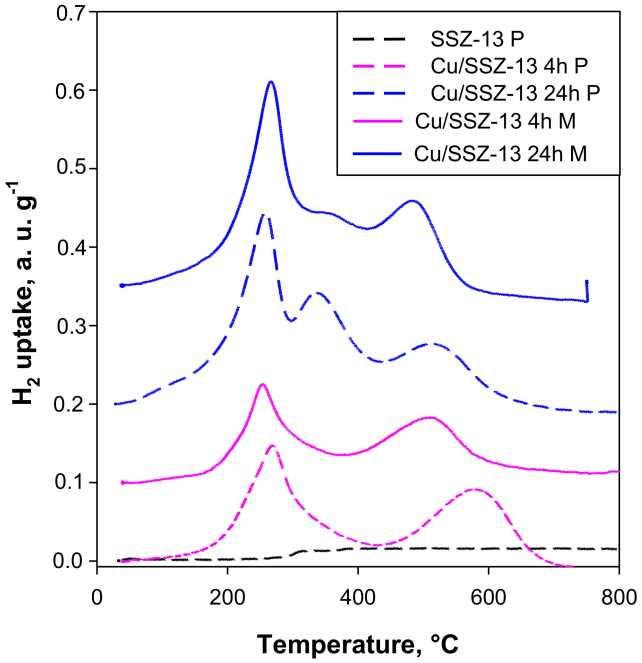

Figure 6. H_2-TPR profiles of Cu/SSZ-13 powders and composite monoliths, exchanged for 4 or 24 h, compared with the TPR profile of the parent SSZ-13.

The total H_2 consumption during TPR is reported in Table 2 together with the corresponding metal contents, estimated under the assumption of complete reduction of Cu(II) to Cu(0). Those values do not always correspond to the results from ICP-MS analysis, but they follow the same increasing trend with the exchange time.

The presence of two well-defined peaks suggests that there are two main different copper species or that a single copper species is reduced into two steps. However, there is a general agreement in the literature regarding the presence of at least two types of copper species in the SSZ-13 framework; the different areas of the two signals are in contrast with a two step reduction of a Cu^{2+} species (from Cu^{2+} to Cu^{+} and from Cu^{+} to Cu^{0}) [7]; however, they should correspond to copper located at different sites. The less easily reducible one, requiring higher temperatures, is located in the 6-MRs, whereas the more reducible copper species is located in the larger 8-MR-sized windows of the chabazite cages [7,15].

Furthermore, Chen et al. [17] found a large signal peaked at about 250 °C, which they assigned to the reduction of isolated copper ions in the form of $[Cu(OH)]^{+}$-Z seated at the 8-MR window site, whilst they attributed a maximum peak of about 360 °C to Cu^{2+}-2Z ions seated at the 6-MR sites.

Similarly, Liu et al. [15] assigned the peak below 300 °C to the reduction of isolated Cu^{2+} species in chabazite cages; however, the peak occurring between 300 and 400 °C was assigned to the reduction of CuO species to Cu^{0}, and the one cantered between 400 and 500 °C was assigned to the reduction of isolated Cu^{2+} ions located in 6-MRs. Eventually, Cu^{+} ions could be reduced at even higher temperatures (>500 °C).

Kwak et al. [1] noticed that the intensity of the low temperature H_2-consumption peak increased with increasing Cu loading, while that higher temperature remained unchanged at Cu ion exchange levels ≥40%. They also proposed that the first Cu ions introduced into the zeolite tend to occupy the most stable and less easily reducible cationic sites (i.e., the six-membered ring-sized ones), whereas, after saturation of these sites, Cu^{2+} ions can then occupy sites inside the larger cages of the CHA structure. These results highlight that the distribution of the two different Cu^{2+} species present in SSZ-13 changes with Cu loading.

On the basis of these attributions, we reasonably assume that the first peak, common to all samples regardless of the exchange time and presence of the silica binder, is related to Cu^{2+} in the 8-MR chabazite cage. The amount of copper located in this position only

slightly increases by increasing the exchange time for the powder sample, whereas a more marked enhancement was observed for the monolith, likely related to a slower penetration rate within the zeolite framework in the presence of the binder. A preliminary TPR test on a reference sample containing only Cu deposited in the silica–laponite matrix (no zeolite) showed almost no contribution.

The assignment of the signals at higher temperatures is more difficult: it can be argued that the intermediate TPR peak is most probably related to extra-framework CuO species, which are more abundant in the pure zeolite powder samples. Indeed, having already saturated the theoretical capacity of the zeolite after 4 h of exchange, any additional Cu can only be located outside of the framework. Eventually, the high temperature reduction is consistent with stable copper ions located in the 6-MRs of the SSZ-13. Accordingly, the presence of the binder surrounding zeolitic crystals appears to contrast and limit the extent of extra-framework copper in 3D composite monoliths, while also preserving easy access to the micropores.

NH_3-TPD profiles, reported in Figure 7, confirm that 3D monolith samples display a surface acidity very similar to that of powder zeolites, considering the smaller fraction of SSZ-13 in the composite material. The amount of NH_3 desorbed, evaluated from the integration of TPD trace, is reported in Table 2, and provides a quantitative check that the values calculated for monolith samples are very close to 60% of those evaluated for powder zeolites for both exchange times, indicating a negligible contribution of the silica-based binder to the ammonia adsorption.

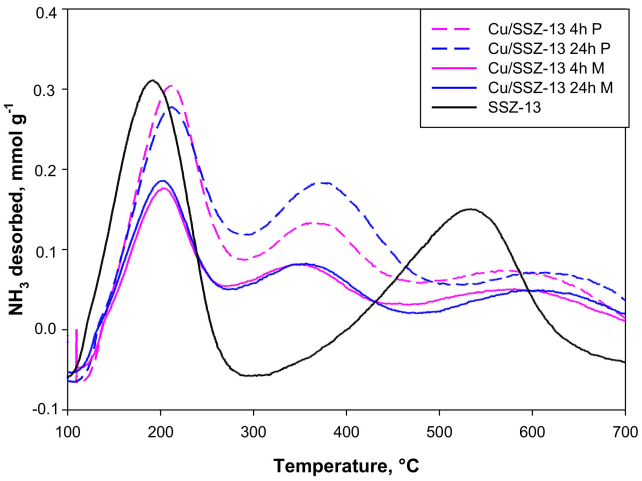

Figure 7. NH_3-TPD profiles of Cu/SSZ-13 both as powder and monoliths, exchanged for 4 or 24 h, compared with the TPR profile of the parent SSZ-13.

All NH_3-TPD profiles of exchanged materials show three desorption signals, with the first one peaking at 202–210 °C, the intermediate one peaking at ca 355–375 °C, while the high temperature peak is rather broad, extending from 500 up to 700 °C for powders and monoliths.

Fan et al. [2] found, for fresh Cu/SSZ-13, a main low-temperature desorption peak located at 190 °C and two small desorption peaks at 320 °C and 400 °C. They associated the low-temperature peak to the weakly bound NH_3 desorbed from Lewis acid sites, whilst the desorption peaks at 320 °C and 400 °C were attributed to the NH_3 adsorbed on strong Lewis acid sites, created by the isolated Cu^{2+} ions and strongly bound NH_3 on Brønsted acid sites, respectively.

Accordingly, Wang et al. [24] reported the presence of three peaks at 97, 345, and 421 °C. On the other hand, after adsorbing ammonia at 100 °C, Wang et al. [30], found only two peaks at ca 250 °C and 420 °C, associated with NH_3 desorbed from Lewis acid sites (Cu^{2+} ions) and from Brønsted acid sites (Si-O(H)-Al), respectively. The attribution of the two peaks at higher temperatures are in agreement with DRIFT results reported by

Zhao et al. [31], who detected molecular NH_3 adsorbed onto Lewis acid sites by Cu^{2+} ions at 1623 cm^{-1} and NH^{4+} formed on Brønsted acid sites at 1465/1482 cm^{-1}. In conclusion, according to these attributions, the desorption event at intermediate temperature can be unambiguously associated with copper species, as also confirmed by its absence in the TPD of the reference SSZ-13 (Figure 7). Furthermore, the more weakly bound ammonia appears to be related to the zeolite structure since the low temperature peak also appeared in the TPD of unexchanged zeolites with roughly the same intensity. Eventually, the strong Brønsted acid sites (Si-O(H)-Al), which are present in large amount in the pristine SSZ-13 zeolite, represent exchangeable sites for copper since the high temperature desorption signal became very weak for all Cu/SSZ catalysts.

Concerning the nature of the copper species associated with the intermediate signal, it is reported [3] that, compared to Cu^{2+}-2Z, $[Cu(OH)]^{+}$-Z is more readily reducible by NH_3 to form $Cu(NH_3)^{n+}$ and H_2O, and that it plays a pivotal role in the NH_3-SCR reaction.

2.3. NH_3-SCR Tests

Exchanged monoliths were tested under conditions described in §3.3, achieving 100% NO conversion from about 150 to 400 °C. However, due to the significantly higher amount of zeolite in the reactor when using monoliths and to some flow limitations of the lab-scale rig, it was not possible to directly compare composite 3D monoliths and their corresponding pure zeolite catalysts at the same gas hourly space velocity. Therefore, 3D monoliths were grounded, and SCR tests were repeated using the same weight and particles size as for the corresponding samples of the pure Cu-SSZ-13 catalyst. In Figure 8, the NO_x conversion as function of the reaction temperature is reported for both the pure zeolites ion-exchanged for 4 and 24 h and their corresponding composite samples derived from monoliths. A blank run over the SSZ-13 powder confirmed a negligible contribution of the pristine zeolite and the key role of the metal active sites. On the other hand, the very low NO_x conversion of the Cu-exchanged binder without zeolite confirmed the active role of copper exchanged into zeolite positions. Roughly 100% NO_x conversion was achieved over all the Cu-exchanged SSZ-13 samples (both as pure and in combination with the binder) in the 200–300 °C temperature range, which is in good agreement with the average NO_x conversion reported by others for Cu-SSZ-13 catalysts in the same range of temperature [26,30,32]. The pure zeolite sample exchanged for only 4 h provided slightly better performance when compared to its counterpart exchanged for 24 h, despite its lower copper load. The decline of NO_x conversion for temperature beyond ca 320 °C was mostly associated with the direct NO oxidation to NO_2 (shown in Figure 8b for Cu/SSZ-13 P 24 h). On the other hand, N_2O production remained below 20 ppm and progressively decreased above 200 °C. It was verified by independent NO adsorption tests under NO/O_2 mixture at 100 °C followed by heating under inert flow that the emission of NO_2 at 300–400 °C occurred by direct NO oxidation. In other words, the Cu/zeolite is able to oxidize pre-adsorbed NO at high temperatures; however, in the presence of NH_3, this unwanted side reaction is limited by the prevailing of the SCR reaction.

In Figure 9, the Arrhenius plots for the NO consumption rate on pure Cu/SSZ-13 powders and composite monoliths are compared to corresponding data for a Cu/binder sample. The domain of the kinetic regime is confirmed by the linear trend of the experimental data obtained in the low to moderate conversion range.

In order to quantitatively confirm the enhanced intrinsic activity of Cu-SSZ-13 within the mesoporous binder, Table 3 reports the values of the apparent activation energy and of the kinetic constant, evaluated at 150 °C per unit mass of catalyst and of zeolite content in the sample; kinetic constants were calculated on the basis of integral reactor conversion data, assuming an ideal isothermal plug flow behaviour and a first-order dependency on NO concentration [26,33].

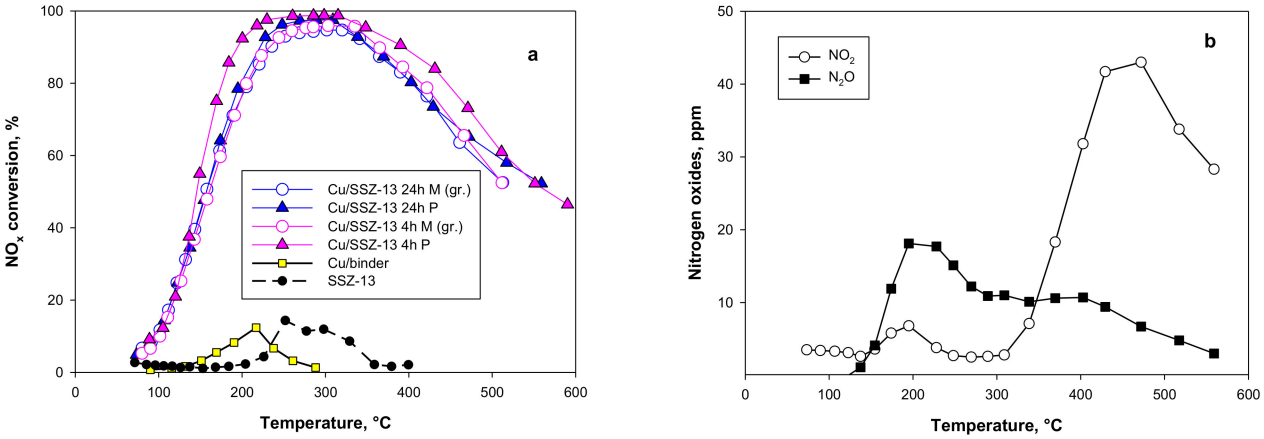

Figure 8. (**a**) NO_x conversion as a function of reaction temperature for copper exchanged (4 and 24 h) SSZ-13 powder and monolith compared with reference materials (Cu/binder and SSZ-13); (**b**) NO_2 and N_2O produced during the activity test over Cu/SSZ-13 P 24 h (Experimental conditions: Catalyst weight = 0.125 g; NO = NH_3 = 400 ppmv, 6% O_2; total flow rate = 25 Sdm^3 h^{-1}).

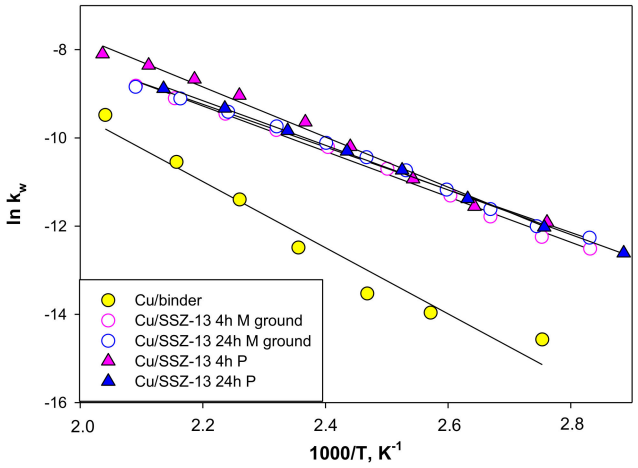

Figure 9. Arrhenius plots for the NO consumption rate per gram of catalyst during the NH_3-SCR of NO on Cu/SSZ-13 powders and monoliths and reference Cu/binder.

Table 3. Apparent activation energy (Ea) and first-order kinetic constant values for the NO removal rate by NH_3-SCR at 150 °C (k_w) per unit mass of catalyst and per unit mass of zeolite (k_{wzeol}) contained in the sample.

Catalyst	Ea (kJ mol^{-1})	$k_{wcatalyst}$ (cm^3 g^{-1} s^{-1})	k_{wzeol} (cm^3 g^{-1} s^{-1})
Cu/binder	62	4.96	-
Cu-SSZ-13 4 h P	49	58.9	58.9
Cu-SSZ-13 24 h P	42	45.2	45.2
Cu-SSZ-13 4 h M	46	44.7	74.5
Cu-SSZ-13 24 h M	44	49.4	82.3

As expected, the reference Cu/binder has a higher activation energy and a kinetic constant one order of magnitude lower than the values associated with Cu-SSZ-13 catalysts. The calculated values of the apparent reaction energy (Ea) of both monoliths and powders fall in quite a narrow range, as is in agreement with values reported for Cu/SSZ-13 by others [26,32], and lower than those evaluated for Cu/ZSM-5 (powder and monolith [23]),

thus confirming the higher activity at lower temperatures for the SSZ-13-based catalyst with respect to ZSM-5 counterparts.

Notably, the intrinsic activity of the zeolite catalyst is higher when the SSZ-13 is incorporated into the silica matrix, as shown by the larger values of k_{wzeol} (last column in Table 3). In other words, both monoliths display a k_w referred to the total sample weight, which is higher than that expected summing up the two contributions proportional to the corresponding fraction of the components in the catalyst. A similar result was previously reported for a Cu/ZSM-5 in a geopolymer matrix [23], once again highlighting the positive effect of a hierarchical porosity on the SCR kinetics, rather than of a different nature of copper sites that, as shown by TPR and TPD analyses, seems to be not modified by the presence of the silica binder.

3. Materials and Methods

3.1. Catalysts Preparation

NH_4-exchanged SSZ-13 (SiO_2/Al_2O_3 = 25) was supplied by Tosoh Corporation (Tokyo, Japan) and preliminary deammoniated under He flow 3 h at 550 °C to obtain H/SSZ-13.

Zeolite-containing slurries were prepared from 59.29 wt% H-SSZ-13 powder, 35.57 wt% colloidal SiO_2 (LUDOX TM-50, Sigma-Aldrich, St. Louis, MO, USA), 3.95 wt% Laponite (Laponite-RD, BYK, Wesel, Germany), and 1.19 wt% carboxymethylcellulose (CMC Na-salt, Sigma-Aldrich, St. Louis, MO, USA) on a dry weight basis; after calcination, the composite consists of 60 wt% SSZ-13, 36 wt% SiO_2, and 4 wt% Laponite. Viscosity was adjusted by dilution with DI water, yielding an overall solid/liquid ratio of 1.53.

Slurries for control samples (without zeolite) were instead prepared from 87.38 wt% colloidal SiO_2, 9.71 wt% Laponite, 2.91 wt% CMC (dry weight basis), and DI water with an overall slurry/liquid ratio of 0.66, yielding a composite of 90 wt% SiO_2 and 10 wt% Laponite after calcination.

Slurry homogenisation was carried out on a high-energy planetary mixer (ARE-250, Thinky Corporation, Chiyoda, Japan) for five cycles (5 min, 2000 rpm) alternated by 5 min sonication cycles in an ultrasound bath. The slurries were allowed to cool down to room temperature after each mixing cycle.

The resulting homogenous pastes were 3D printed by Direct Ink Writing at room temperature on a Delta-type 3D printer (Delta 2040 Turbo, WASP, Massa Lombarda, Italy). The material was fed into the chamber of an auger-type extruder (LDM extruder 3.0, WASP, Massa Lombarda, Italy) via pneumatic pressure, from which it was extruded through an 840 µm tapered nozzle (VIEWEG GmbH, Kranzberg, Germany) with 630 µm layer height and 30 mm s^{-1} printing speed. 3D-printing toolpaths were generated through a custom algorithm implemented in the Rhinoceros/Grasshopper CAD software (Ver. 7 SR23, TLD Inc., Windsor, CT, USA) to produce cylindrical samples (Ø 19.5 mm, H 12.5 mm) with a log-pile scaffold configuration and 50% nominal design porosity.

Following Direct Ink Writing (DIW), the samples were dried for 24 h at 40 °C, and subsequently calcined at 550 °C (4 h, 5 °C min^{-1} heating ramp) in still air to remove the organic fraction and induce partial sintering of the SiO_2 nanoparticles.

An early attempt to embed the SSZ-13 into a geopolymer matrix, as already completed for ZSM-5, resulted in a very low mechanical resistance of the monolith and in the almost total loss of the crystalline structure of SSZ-13, as described in Section 2.

Before copper exchange, the 3D-printed monoliths were pre-treated in a HNO_3 aqueous solution to achieve a neutral pH, as described in [22,23], and then calcined for 4 h at 550 °C.

Then, copper was exchanged starting from a copper acetate solution (0.02 M) for 4 h or 24 h at 80 °C with a zeolite/solution volume ratio of 8 g/L for both powder and monolith SSZ-13. After the exchange, the monolith was calcined at 400 °C for 2 h.

Reference monolith samples containing 100% binder were also prepared and treated with HNO_3 then with copper solution, following the same procedure applied for monoliths exchanged for 4 h.

3.2. Catalysts Characterization

SEM analysis was carried out using an FEI Inspect scanning electron microscope (FEI Electron Optics, Eindhoven, The Netherlands).

Specific surface area measurements and micro/meso-pore analyses were performed in an Autosorb 1-C (Quantachrome Instruments, Boynton Beach, FL, USA) through N_2 adsorption at 77 K after degassing the samples for 12 h at 150 °C. The specific surface area and the pore size distribution were evaluated by the BET and NLDFT methods, respectively. The total pore volume was estimated by Gurvitch method.

The actual copper loading of both powder and monolith samples was evaluated by ICP-MS using an Agilent 7500 instrument (Santa Clara, CA, USA) after dissolving the samples in HF solution.

H_2-TPR analysis was carried out with a AutoChem 2020 (Micromeritics, Norcross, GA, USA) equipped with a TC detector. Catalyst samples (150 mg) were pre-treated in situ under air flow at 400 °C for 1 h; thereafter, 2% vol. H_2/Ar mixture (50 cm^3 min^{-1}) was passed through the sample, heating from room temperature up to 800 °C at 10 °C min^{-1}.

NH_3-TPD experiments were conducted with the same apparatus, pre-treating the catalyst at 250 °C (0.5 h) under He flow, cooling down to 100 °C, and saturating the sample at this temperature with a NH_3/He mixture for 1 h. Thereafter, ammonia was desorbed via heating up to 750 °C at 10 °C/min under He flow (50 cm^3 min^{-1}).

3.3. Catalytic Tests

SCR catalytic tests were carried out in the experimental rig described in [23] using a packed bed of powdered catalysts (0.125 g, 125–250 μm). To this aim, 3D composite monoliths were grounded and sieved to the desired size range before testing. The gas feed was obtained by mixing gas streams from high purity cylinders (1% NO in He, 0.4% NH_3 in He, O_2, He) (Air Liquide, Milano, Italy), regulated by independent, dent mass flow controllers (BROOKS MFC SLA5850S) (Brooks Instruments, Dresden, Germany) in order to achieve an inlet gas composition of NO = NH_3 = 400 ppmv (NO_2 impurity < 4 ppmv), 6% O_2. The total flow rate was fixed at 25 Sdm^3 h^{-1}, and the operating temperature ranged from 70 to 550 °C.

Catalytic tests under the same feed conditions were also repeated over 3D monoliths (d = 18 mm, l = 20 mm, average weight = 1.7 g), which were wrapped with a ceramic tape and placed into a tubular quartz reactor (d_{in} = 20 mm) [23,33].

Analysis of nitrogen oxides was performed by a continuous analyser for NO, N_2O (ND-IR), and NO_2 (UV) Emerson X-Stream XEGP (Emerson, Bussero (MI), Italy). Water and NH_3 from the product gas stream were removed using a Sycapent™ (P_2O_5) (Sigma-Aldrich, St. Louis, MO, USA) before entering the NO_x analyser.

4. Conclusions

Through an additive manufacturing approach, we successfully prepared 3D-structured monolith catalysts by embedding up to 60% weight fraction of a commercial SSZ-13 zeolite into a mesoporous SiO_2 matrix to provide both mechanical stability and hierarchical porosity. In particular, it was found that the use of silica as a binder preserved the SSZ-13 zeolite structure, as opposed to the more aggressive (strongly basic) precursors that were previously employed to produce a geopolymer matrix to embed the zeolite.

The addition of a small fraction of laponite into a silica matrix improved the mechanical stability during all the steps of a 3D-printing process by Direct Ink Writing. Ion exchange with copper was investigated to prepare active catalysts for the NH_3-SCR of NO. A prolonged copper exchange resulted in the introduction of additional inactive metal, likely not located in the main exchange positions. This effect is more evident for pure zeolite catalysts; however, it is favourably contrasted by the presence of the silica binder, which limits the undesired over-exchange phenomenon in monolith catalysts.

The main textural, acid, and redox properties of the SSZ-13 are preserved in the 3D monoliths with a negligible contribution of the binder that uniformly covers SSZ-13

particles without occluding pores, changing the nature of the copper, or neutralizing acid sites that were identified in the pristine Cu-SSZ-13. However, the binder plays a fundamental role, not only providing the required mechanical stability to the structured zeolite, but also enhancing the catalytic performance, thanks to the hierarchical porosity created by the intimate contact between the mesoporous silica and the microporous SSZ-13. While avoiding the common drawbacks of high pressure drops related to the use of a packed bed of particle catalysts, 3D-printed composite monoliths can outperform standard zeolite-wash coated honeycombs due to their higher loading of active phase, hierarchical porosity, and enhanced mass transfer coefficients.

In summary, the enhanced hydrothermal stability and sulphur tolerance of SSZ-13 relative to other SCR-active zeolites, coupled with the improved catalytic performance observed for Cu-exchanged 3D-printed silica/SSZ-13 monoliths, render these structured materials promising candidates for SCR applications in diesel engine exhaust treatment.

Author Contributions: Conceptualization, L.L., S.C. and G.F.; investigation, E.M.C., M.D. and G.F.; data curation, E.M.C. and M.D.; writing—original draft preparation, L.L.; writing—review and editing, S.C., G.F. and N.G.; visualization, S.C. and N.G.; supervision, L.L.; funding acquisition, L.L., G.F. and E.M.C. All authors have read and agreed to the published version of the manuscript.

Funding: This research was partially funded by Ministero Università e Ricerca—Italy (PRIN 2017PMR932) and European Union—NextGenerationEU under the National Recovery and Resilience Plan (NRRP), Mission 04 Component 2 Investment 3.1, Project Code: IR0000027-CUP:B33C22000710006-iENTRANCE@ENL: Infrastructure for Energy TRAnsition aNd Circular Economy @ EuroNanoLab.

Data Availability Statement: Data are contained within the article.

Conflicts of Interest: The authors declare no conflicts of interest.

References

1. Kwak, J.A.; Zhu, H.; Lee, J.H.; Peden, C.H.F.; Szanyi, J. Two different cationic positions in Cu-SSZ-13? *Chem. Commun.* **2012**, *48*, 4758–4760. [CrossRef] [PubMed]
2. Fan, C.; Chen, Z.; Pang, L.; Ming, S.; Dong, C.; Albert, K.B.; Liu, P.; Wang, J.; Zhu, D.; Chen, H.; et al. Steam and alkali resistant Cu-SSZ-13 catalyst for the selective catalytic reduction of NO_x in diesel exhaust. *Chem. Eng. J.* **2018**, *334*, 344–354. [CrossRef]
3. Shan, Y.; Du, J.; Zhang, Y.; Shan, W.; Shi, X.; Yu, Y.; Zhang, R.; Meng, X.; Xiao, F.-S.; He, H. Selective catalytic reduction of NO_x with NH_3: Opportunities and challenges of Cu-based small-pore zeolites. *Natl. Sci. Rev.* **2021**, *8*, nwab010. [CrossRef] [PubMed]
4. Putluru, S.S.R.; Riisager, A.; Fehrmann, R. Alkali resistant Cu/zeolite deNO_x catalysts for flue gas cleaning in biomass fired applications. *Appl. Catal. B Environ.* **2011**, *101*, 183–188. [CrossRef]
5. Chen, B.; Xu, R.; Zhang, R. Economical way to synthesize SSZ-13 with abundant ion-exchanged Cu^+ for an extraordinary performance in selective catalytic reduction (SCR) of NO_x by ammonia. *Environ. Sci. Technol.* **2014**, *48*, 13909–13916. [CrossRef] [PubMed]
6. Stewart, M.L.; Kamp, C.J.; Gao, F.; Wang, Y.; Engelhard, M.H. Coating Distribution in a Commercial SCR Filter. *Emiss. Control Sci. Technol.* **2018**, *4*, 260–270. [CrossRef]
7. Ma, L.; Cheng, Y.; Cavataio, G.; McCabe, R.W.; Fu, L.; Li, J. Characterization of commercial Cu-SSZ-13 and Cu-SAPO-34 catalysts with hydrothermal treatment for NH_3-SCR of NO_x in diesel exhaust. *Chem. Eng. J.* **2013**, *225*, 323–330. [CrossRef]
8. Paolucci, C.; Di Iorio, J.R.; Ribeiro, F.H.; Gounder, R.; Schneider, W.F. Chapter One—Catalysis Science of NO_x Selective Catalytic Reduction with Ammonia Over Cu-SSZ-13 and Cu-SAPO-34. In *Advances in Catalysis*; Academic Press: Cambridge, MA, USA, 2016; Volume 59, pp. 1–107.
9. Song, J.; Wang, Y.; Walter, E.D.; Washton, N.M.; Mei, D.; Kovarik, L.; Engelhard, M.H.; Prodinger, S.; Wang, Y.; Peden, C.H.F.; et al. Toward Rational Design of Cu/SSZ-13 Selective Catalytic Reduction Catalysts: Implications from Atomic-Level Understanding of Hydrothermal Stability. *ACS Catal.* **2017**, *7*, 8214–8227. [CrossRef]
10. Luo, J.; Gao, F.; Kamasamudram, K.; Currier, N.; Peden, C.H.F.; Yezerets, A. New insights into Cu/SSZ-13 SCR catalyst acidity. Part I: Nature of acidic sites probed by NH_3 titration. *J. Catal.* **2017**, *348*, 291–299. [CrossRef]
11. Daya, R.; Trandal, D.; Dadi, R.K.; Li, H.; Joshi, S.Y.; Luo, J.; Kumar, A.; Yezerets, A. Kinetics and thermodynamics of ammonia solvation on Z2Cu, ZCuOH and ZCu sites in Cu-SSZ-13—Implications for hydrothermal aging. *Appl. Catal. B Environ.* **2021**, *297*, 120444. [CrossRef]
12. Jangjou, Y.; Do, Q.; Gu, Y.; Lim, L.-G.; Sun, H.; Wang, D.; Kumar, A.; Li, J.; Grabow, L.C.; Epling, W.S. Nature of Cu Active Centers in Cu-SSZ-13 and Their Responses to SO_2 Exposure. *ACS Catal.* **2018**, *8*, 1325–1337. [CrossRef]
13. Du, J.; Shan, Y.; Sun, Y.; Gao, M.; Liu, Z.; Shi, X.; Yu, Y.; He, H. Unexpected increase in low-temperature NH_3-SCR catalytic activity over Cu-SSZ-39 after hydrothermal aging. *Appl. Catal. B Environ.* **2021**, *294*, 120237. [CrossRef]

14. Ma, Y.; Cheng, S.; Wu, X.; Ma, T.; Liu, L.; Jin, B.; Liu, M.; Liu, J.; Ran, R.; Si, Z.; et al. Improved hydrothermal durability of Cu-SSZ-13 NH_3-SCR catalyst by surface Al modification: Affinity and passivation. *J. Catal.* **2022**, *405*, 199–211. [CrossRef]
15. Liu, B.; Lv, N.; Wang, C.; Zhang, H.; Yue, Y.; Xu, J.; Bi, X.; Bao, X. Redistributing Cu species in Cu-SSZ-13 zeolite as NH_3-SCR catalyst via a simple ion-exchange. *Chin. J. Chem. Eng.* **2022**, *41*, 329–341. [CrossRef]
16. Peng, C.; Yan, R.; Peng, H.; Mi, Y.; Liang, J.; Liu, W.; Wang, X.; Song, G.; Wu, P.; Liu, F. One-pot synthesis of layered mesoporous ZSM5 plus Cu ion-exchange: Enhanced NH_3-SCR performance on Cu-ZSM5 with hierarchical pore structures. *J. Hazard. Mater.* **2020**, *385*, 121593. [CrossRef] [PubMed]
17. Chen, Z.; Ye, T.; Qu, H.; Zhu, T.; Zhong, Q. Progressive regulation of Al sites and Cu distribution to increase hydrothermal stability of hierarchical SSZ-13 for the selective catalytic reduction reaction. *Appl. Catal. B Environ.* **2022**, *303*, 120867. [CrossRef]
18. Wijayanti, K.; Xie, K.; Kumar, A.; Kamasamudram, K.; Olsson, L. Effect of gas compositions on SO_2 poisoning over Cu/SSZ-13 used for NH_3-SCR. *Appl. Catal. B Environ.* **2017**, *219*, 142–154. [CrossRef]
19. Wijayanti, K.; Leistner, K.; Chand, S.; Kumar, A.; Kamasamudram, K.; Currier, N.W.; Yezerets, A.; Olsson, L. Deactivation of Cu-SSZ-13 by SO_2 exposure under SCR conditions. *Catal. Sci. Technol.* **2016**, *6*, 2565–2579. [CrossRef]
20. Lisi, L.; Pirone, R.; Russo, G.; Stanzione, V. Cu-ZSM5 based monolith reactors for NO decomposition. *Chem. Eng. J.* **2009**, *154*, 341–347. [CrossRef]
21. Nova, I.; Bounechada, D.; Maestri, R.; Tronconi, E.; Heibel, A.K.; Collins, T.A.; Boger, T. Influence of the substrate properties on the performances of NH_3-SCR monolithic catalysts for the aftertreatment of diesel exhaust: An experimental and modeling study. *Ind. Eng. Chem. Res.* **2011**, *50*, 299–309. [CrossRef]
22. Cepollaro, E.M.; Cimino, S.; Lisi, L.; Botti, R.; Colombo, P.; Franchin, G. Cu-exchanged 3D-printed Geopolymer/ZSM-5 Monolith for Selective Catalytic Reduction of NO_x. *Chem. Eng. Trans.* **2021**, *84*, 67–72.
23. Cepollaro, E.M.; Botti, R.; Franchin, G.; Lisi, L.; Colombo, P.; Cimino, S. Cu/ZSM5-Geopolymer 3D-Printed Monoliths for the NH_3-SCR of NO_x. *Catalysts* **2021**, *11*, 1212. [CrossRef]
24. Wang, Z.; Xu, X.; Zhu, Y.; He, H.; Wang, N.; Yang, X.; Liu, L. One-pot synthesis of hierarchical MnCu-SSZ-13 catalyst with excellent NH_3-SCR activity at low temperatures. *Microporous Mesoporous Mater.* **2022**, *333*, 111720. [CrossRef]
25. Thommes, M.; Cychosz, K. Physical adsorption characterization of nanoporous materials: Progress and challenges. *Adsorption* **2014**, *20*, 233–250. [CrossRef]
26. Kwak, J.H.; Tran, D.; Szanyi, J.; Peden, C.H.F.; Lee, J.H. The Effect of Copper Loading on the Selective Catalytic Reduction of Nitric Oxide by Ammonia Over Cu-SSZ-13. *Catal. Lett.* **2012**, *142*, 295–301. [CrossRef]
27. Clemens, A.K.S.; Shishkin, A.; Carlsson, P.-A.; Skoglundh, M.; Martínez-Casado, F.J.; Matěj, Z.; Balmes, O.; Härelind, H. Reaction-driven Ion Exchange of Copper into Zeolite SSZ-13. *ACS Catal.* **2015**, *5*, 6209–6218. [CrossRef]
28. Delavernhe, L.; Pilavtepe, M.; Emmerich, K. Cation exchange capacity of natural and synthetic hectorite. *Appl. Clay Sci.* **2018**, *151*, 175–180. [CrossRef]
29. Khurana, I.; Albarracin-Caballero, J.D.; Shih, A.J. Identification and quantification of multinuclear Cu active sites derived from monomeric Cu moieties for dry NO oxidation over Cu-SSZ-13. *J. Catal.* **2022**, *413*, 111–1122. [CrossRef]
30. Wang, C.; Wang, J.; Wang, J.; Wang, Z.; Chen, Z.; Li, X.; Shen, M.; Yan, W.; Kang, X. The Role of Impregnated Sodium Ions in Cu/SSZ-13 NH_3-SCR Catalysts. *Catalysts* **2018**, *8*, 593. [CrossRef]
31. Zhao, H.; Yang, G.; Hill, A.J.; Luo, B.; Jing, G. One-step ion-exchange from Na-SSZ-13 to Cu-SSZ-13 for NH_3-SCR by adjusting the pH value of Cu-exchange solution: The effect of H^+ ions on activity and hydrothermal stability. *Microporous Mesoporous Mater.* **2021**, *324*, 111271. [CrossRef]
32. Cui, Y.; Wang, Y.; Walter, E.D.; Szanyi, J.; Wang, Y.; Gao, F. Influences of Na^+ co-cation on the structure and performance of Cu/SSZ-13 selective catalytic reduction catalysts. *Catal. Today* **2020**, *339*, 233–240. [CrossRef]
33. Gargiulo, N.; Caputo, D.; Totarella, G.; Lisi, L.; Cimino, S. Me-ZSM-5 monolith foams for the NH_3-SCR of NO. *Catal. Today* **2018**, *304*, 112–118. [CrossRef]